HPV oncogenes increase viability and nuclear architecture stability in pretumoral keratinocytes exposed to UVB radiation

Magdalena Millán
Universidad de La República
Felipe Parietti
Universidad de La República
Paola Hernández
Instituto de Investigaciones Biológicas Clemente Estable, Ministerio de Educación y Cultura
Sofía Yocco
Universidad de La República
Jorge Pérez-Zerpa
University of the Republic
Miguel Arocena
Universidad de La República
Jimena Hochmann
jimehoc@gmail.com

Universidad de La República

Short Report

Keywords: HPV-18 oncogenes, DNA damage, nuclear architecture, UVB radiation

Posted Date: December 15th, 2025

DOI: https://doi.org/10.21203/rs.3.rs-8272583/v1

Additional Declarations: No competing interests reported.

Abstract

Ultraviolet radiation (UVR) is an environmental risk factor and a cofactor in carcinogenesis. UVB radiation (UVBR), mainly from sunlight, is a known risk factor for lip cancer and can also contribute to oral cavity cancer. Besides inducing DNA damage, UVBR can activate dormant HPV infections in the oral cavity, increasing oral carcinogenesis likelihood via HPV oncogenes. In this study, we evaluated the responses to UVBR in human keratinocytes infected with viral oncogenes of HPV-18. While UVBR induced similar levels of DNA damage in the HaCaT human keratinocyte parental cell line compared to HaCaT cells containing HPV-18 oncogenes E5, E6 and E7, the latter showed increased viability and reduced levels of apoptotic and necrotic markers in response to UVBR. Both HaCaT parental and HaCaT E5/E6/E7-18 cells showed marked alterations in the actin cytoskeleton upon UVBR, but HaCaT parental cells retained more stress fibers, while displaying deep nuclear invaginations, which were much less frequent in HaCaT E5/E6/E7-18 cells. Deep nuclear invaginations were lined by highly condensed chromatin, implying alterations in nuclear architecture that profoundly affect normal nuclear compartmentalization. Furthermore, mechanical modelling suggests that reduced nuclear invaginations in irradiated HaCaT E5/E6/E7-18 cells is related to decreased tractional stress. Our results show that HPV oncogenes confer increased viability and nuclear architecture stability to keratinocytes exposed to UVBR, which could contribute to their role in cooperating with UVBR induced carcinogenesis in the oral cavity.

Introduction

Solar ultraviolet radiation (UVR) is a human carcinogen, particularly in the UVB range of the spectrum (Kumar et al., 2015). UVB plays a variety of roles in the induction of skin cancers, but it could also affect internal oral tissues as it is used during various dental diagnostic and treatment procedures (Bush et al., 2010; McGee et al., 2008). Therefore, UVR could be considered a risk factor in the development of oral cancer. UVB generates dimeric photoproducts between adjacent pyrimidine bases, but it can also lead to double strand break (DSB) induction, followed by cell-cycle arrest and cell death (Azzouz et al.,2018; Greinert R et al., 2012). Furthermore, UVR contributes to tumorigenesis since it can activate viruses such as human papillomavirus (HPV), and HPV oncogenes can further contribute to the survival and proliferation of mutated cells (Leverrier et al., 2007; Jackson et al., 2000).

Together with UVB radiation, HPVs of the beta genus could act as a cofactor promoting skin cancer (Minoni et al., 2020). HPVs of the alpha genus, such as high risk types 16 and 18, are involved in oral carcinogenesis, particularly in oropharyngeal cancer (Kreimer et al., 2005). While their interaction with UVR during the process of tumorigenesis is less well studied than for beta HPVs, there is evidence that both cooperate to drive oral carcinogenesis. For example, oropharyngeal cancer risk is associated both to alpha HPV infection and to UVR (Godar et al., 2014). Lip squamous cell carcinoma is a type of oral carcinoma where association with UVR is well established, and is frequently positive for alpha HPV infection (Hassouna et al., 2019), underscoring the potential for alpha HPV oncogenes and UVR in cooperating to drive oral carcinogenesis. Therefore, studying how keratinocytes expressing alpha HPV

oncogenes respond to radiation is important to gain insights into the process of oral carcinogenesis induced by UVBR in cooperation with high risk HPV infection.

Cellular and nuclear architecture are fundamental parameters in determining cell viability, and they can be altered both by UVR and by viral oncogenes. Nuclear invaginations in particular have been observed in conditions with decreased cell viability. (Tripodis and Demant., 2001; Gartner.,1976). Moreover, UVR has been previously shown to induce nuclear invaginations in cultured cells (Szekely et al., 1980). Regarding viral oncogenes, in our previous study we showed that the HaCaT human keratinocyte cell line transduced with the E5, E6, E7 oncogenes from HPV-18 (HaCaT E5/E6/E7-18) are less rigid and more rounded than their parental counterparts (Millán et al., 2023), highlighting the potential of viral oncogenes to modify cell architecture.

In this study, we have studied the effects of UVB radiation both on HaCaT parental cells and the HaCaT E5/E6/E7-18 cells previously mentioned. We show that, despite similar levels of UVBR induced DNA damage, HaCaT E5/E6/E7-18 cells have increased viability and decreased alterations in nuclear architecture compared to their parental counterparts, suggesting that alpha HPV oncogenes can contribute to UVB induced carcinogenesis in sites such as the oral cavity.

Material and Methods

2.1. Cell culture

Immortalized, non-tumoral HaCaT parental cells and pre-tumoral HaCaT E5/E6/E7 HPV-18 cells, were cultured in DMEM (Capricorn Scientific, Ebsdorfergrund, Germany) supplemented with 10% FBS (Capricorn Scientific, Ebsdorfergrund, Germany) and 1% Penicillin-Streptomycin (Capricorn Scientific, Ebsdorfergrund, Germany) at 37ºC under humidified atmosphere with 5% CO_2. The preparation and characterization of HaCaT E5/E6/E7-18 cells lines was detailed in Hochmann et al., 2020, whereas HaCaT parental cells were obtained from ATCC. For UVB exposure and subsequent microscopy analysis, cells were grown on 35 mm glass bottom dishes in 1.5 ml of complete medium.

2.2 UVB Exposure

The cells were cultured in 35-mm glass-bottom dishes at 1×10^5 cells/well in 1.5 ml of complete medium for exposure to UVB. Cells were incubated for 24 h until they reached a confluence of approximately 70%. Cultures were washed with PBS once, and then 0.5 mL of PBS was added in each well. Then, cells were exposed to 0.05 J/cm^2 UVB (Analytikjena UVLMS-38, 8W, 302 nm) during 8 minutes and 42 seconds.

2.3 Cell Viability Assessment

The MTT method was used to evaluate the impact of UVB radiation on the viability of HaCaT parental and HaCaT E5/E6/E7-18 cells. For this purpose, the cells were cultured in 24-well plates (5×10^4 cells/well). After reaching a confluence of approximately 90%, the cells were washed with PBS once,

after which a volume of 500 µL/well of PBS was added, and the cells were exposed to UVB (0.05 J/cm^2). Immediately after exposure, PBS was replaced with 500 µL of fresh culture medium, 10 µL of MTT (5 mg/mL) reagent was added to each well, and the plates were incubated for 4 h. Then, 120 µL/well of isopropanol was added to each well. When formazan crystals were solubilized, 100 µL were transferred to a 96 well plate. The absorbance was measured at wavelength of 570 nm using a microplate spectrophotometer (Varioskan Flash Microplate spectrophotometer, Thermo Fisher,Waltham, MA, USA).

2.4. Detection of apoptotic and necrotic markers

To assess the presence of necrotic and apoptotic cells, we used Propidium Iodide (PI) and Annexin V dyes, respectively (both from Biotum, San Francisco, USA), at final concentration of 1µM for PI and 0.25 µg/mL for Annexin V.HaCaT parental and HaCaT E5/E6/E7-18 cells were cultured in 35-mm glass-bottom dishes at 1 × 10^5 cells/well in 1.5 ml of complete medium and were incubated with both dyes at room temperature for 15 minutes, and with Hoechst 333142 (dilution 1/1000, Invitrogen) to stain nuclei. Staining with PI and Annexin V was evaluated at time 0 and 24 hours post irradiation with 0.05J/cm^2 of UVB. The images were obtained with the module of epifluorescence of the quantitative phase microscope Nanolive 3D Cell Explorer-Fluo. PI and Annexin V fluorescence positive cells per field were assessed at 24 hours post UVB irradiation in 200 cells per condition using the ImageJ software v. 1.43n4.

2.5 Detection of F actin in live cells

Live Cell Fluorogenic F-actin Labelling Probe (Cytoskeleton, Inc. Denver, CO, USA, final concentration of 1µM) was used to visualize the actin cytoskeleton in HaCaT parental and HaCaT E5/E6/E7-18 cells irradiated with 0.05J/cm^2 UVB and non irradiated controls. The images were obtained with the module of epifluorescence of the quantitative phase microscope Nanolive 3D Cell Explorer-Fluo and analyzed with the software ImageJ. The quantification of cells presenting stress fiber-like filaments was carried out in 50 cells per condition at time 0 and 24 hours post UVB irradiation using the ImageJ software v. 1.43n4.

2.6 Detection of filamentous actin (F-actin) by phalloidin staining

Cells irradiated with 0.05J/cm^2 of UVB, and non irradiated controls, at time 0 and 24 post radiation, were fixed for 10 min in 4% paraformaldehyde, rinsed in PBS three times, 5 min each, and permeabilized with 1% Triton X-100 diluted in PBS for 5 minutes at room temperature. Then, cells were blocked with 1% BSA for 30 minutes at room temperature. Afterwards, permeabilized cells were incubated with Alexa Fluor™ 488 labelled phalloidin (dilution 1/1000, Life Technologies, Massachusetts, USA), and DAPI (dilution 1/1000, Life Technologies, Massachusetts, USA to stain nuclei. Finally, cells were visualized using a Zeiss LSM800 confocal microscope.

2.7 Immunocytochemistry

HaCaT parental and HaCaT E5/E6/E7 HPV-18 irradiated with 0.05J/cm^2 of UVB and non irradiated controls were fixed for 10 min in 4% paraformaldehyde, rinsed in PBS three times, 5 min each, and permeabilized with 1% Triton X-100 diluted in PBS for 5 min at room temperature. Then, cells were blocked with 1% BSA for 30 minutes at room temperature and incubated with their respective primary antibodies: anti-lamin A/C antibody diluted in blocking buffer (dilution 1/200, Lamin A/C (4C11) Mouse mAb; Cell Signaling, Danvers, Massachusetts, USA), and anti-γH2AX antibody diluted in blocking buffer (dilution 1/300, Phospho-Histone H2A.X (Ser139) (20E3) Rabbit mAb; Cell Signaling, Danvers, Massachusetts, USA) overnight at 4°C. Finally, cells were washed with PBS three times for 5 min each, and incubated for an hour with secondary antibody (goat anti-mouse conjugated with Alexa 488 dilution 1:1000, Thermo Fisher Scientific, Waltham, Massachusetts, USA, or goat anti-rabbit conjugated with Alexa488, dilution 1:1000), and DAPI (dilution l/1000) to stain nuclei. Finally, cells were visualized using a Zeiss LSM800 confocal microscope. The γH2AX nuclear fluorescence was quantified in 20 cells per condition using the ImageJ software v. 1.43n4.

2.8 Quantitative phase imaging

HaCaT parental and HaCaT E5/E6/E7 HPV-18 cells, irradiated and non irradiated controls,were imaged with the quantitative phase microscope Nanolive 3D Cell Explorer-Fluo at 0 and 24 hours post UVB irradiation. Nuclear invaginations were quantified at 24 hours post UVB irradiation using the ImageJ software v. 1.43n4.

2.9 Modelling of nuclear invaginations

Cellular membranes, including the nuclear envelope, can be modelled as a membrane structure subjected to the forces given by its interaction with internal components of the cell (Jenkins., 1977). Membrane structures usually are formed by textile elements tensioned by cables. They are able to resist tension forces while they are not able to resist bending moments or compression forces, leading to wrinkles analogous to invaginations (Lewis., 2003). The problem of computing the deformation of membrane structures, also known as form finding, in the context of cellular membranes involves challenges due to the consideration of geometric nonlinearities, fluid pressure, contact with internal structures (Beiter, Voth., 2024). Here, a simplified model of a cellular membrane representing the nuclear envelope is considered in order to provide a conceptual argumentation for the formation of wrinkles analogous to nuclear invaginations. In this simplified model the membrane is modelled as a network of cables interconnected. Specific mathematical techniques have been developed for the computational analysis of structures formed by cables (Kanno., 2011., Zhang et al., 2011). For the computational modelling, an open source library developed in Python called cablenets[1] was developed, for the application of the algorithm presented in (Kanno, Ohsaki., 2003). A square domain is considered as shown in Fig. 5E, where the plane x-y cablenet is subjected to a uniform distributed force in z (green arrows) and imposed displacements D in two vertices (blue arrows), representing the tractional forces experienced by cells and therefore by the nucleus, given its mechanical connection with the rest of the cell (Janota et al., 2020). Membrane deformation is computed, and probable directions for wrinkle formation are computed identifying cable elements without tension.

2.10 Statistical analysis

Statistical analysis and graphical presentation were performed using GraphPad Prism version 8.0.1 software (GraphPad Software Inc., San Diego, CA, USA). All experiments were performed in triplicate, and data were presented as the mean ± standard deviation (SD). For all statistical analysis, two-way analysis of variance (ANOVA) test was conducted to assess statistical significance among groups followed by Tukey's HSD *post-hoc* test, with the exception of nuclear invaginations quantification, which was analyzed using Student`s Test in order to compare only two means. Statistical significance was determined at $p < 0.05$.

Results and Discussion

HaCaT cells expressing HPV-18 oncogenes have increased viability but similar levels of DNA damage than their parental counterparts

HaCaT E5/E6/E7-18 and HaCaT parental cells were irradiated with 0.05J/cm^2 of UVB for 24 hours, and cell viability and apoptotic and necrotic markers were assessed (Fig. 1). Cell viability, measured by the MTT assay, was markedly decreased 24h after UVBR, but, at the same time, HaCaT E5/E6/E7-18 cells retained significantly higher viability than their parental counterparts (Fig. 1A). Consistent with this result, we observed significantly lower levels of HaCaT E5/E6/E7-18 cells positive for apoptotic and necrotic markers (Annexin V and Propidium Iodide, respectively) compared to HaCaT parental cells 24h after UVBR (Fig. 1B,C). We next assessed γH2AX levels as a marker of DNA damage after UVBR. γH2AX levels markedly increased 24h after UVBR exposure, but we did not observe significant differences in γH2AX levels between HaCaT E5/E6/E7-18 and HaCaT parental cells (Fig. 2).

Stress fibers and perinuclear actin rings are affected by UVBR

In our previous work, we showed that HPV oncogenes alter mechanical properties as well as cell architecture in HaCaT cells. We therefore examined the actin cytoskeleton, a fundamental parameter of cell organization, in HaCaT E5/E6/E7-18 and HaCaT parental cells after UVBR. First, we used the SIR-actin live cell probe to assess changes in the cytoskeleton of live HaCaT E5/E6/E7-18 and HaCaT parental cells after UVBR (Fig. 3A). We observed important alterations in the actin cytoskeleton after UVBR, which were more marked in HaCaT E5/E6/E7-18 cells. In particular, the number of HaCaT E5/E6/E7-18 cells that maintained stress fibers 24h after UVBR was significantly reduced compared to HaCaT parental cells in the same condition (Fig. 3B). When we visualized the actin cytoskeleton by phalloidin staining (Fig. 3C), we observed that in control conditions both HaCaT E5/E6/E7-18 and HaCaT parental cells had prominent perinuclear actin rings, previously observed in other cell types (Fracchia et al., 2020). However, 24h after UVBR, perinuclear actin rings completely disappeared in both HaCaT E5/E6/E7-18 and HaCaT parental cells (Fig. 3C).

HPV oncogenes attenuate UVBR induced nuclear invaginations

Using label-free, holotomographic quantitative phase microscopy in live HaCaT E5/E6/E7-18 and HaCaT parental cells, we observed the appearance of marked nuclear lines 24h after UVBR (Fig. 4A and B). Interestingly, however, HaCaT E5/E6/E7-18 cells showed significantly less nuclear lines than HaCaT parental cells (Fig. 4C). Holotomographic quantitative phase microscopy generates 3D images allowing xy and yz reconstructions, which showed that these nuclear lines corresponded to deep nuclear invaginations (Figs. 5A and B). Moreover, nuclear lines observed by quantitative phase microscopy colocalize with lamin A/C signal (Fig. 4B), and nuclear lines also appear clearly in confocal images of lamin A/C 24h after UVBR (Fig. 4D). Furthermore, xy and yz confocal reconstructions of lamin A/C signal similarly show that nuclear lines positive for lamin A/C correspond to deep nuclear invaginations (Figs. 5C and D). These nuclear invaginations are also sites of high chromatin condensation, as evidenced by intense DAPI staining (Figs. 5C and D). Because the number of nuclear invaginations (detected as nuclear lines) is significantly reduced in HaCaT E5/E6/E7-18 cells compared to their parental counterparts (Fig. 4C), we can conclude that HPV oncogenes attenuate the perturbations in nuclear architecture caused by UVBR exposure. Irradiated HaCaT E5/E6/E7-18 cells show reduced stress fibers compared to irradiated HaCaT parental cells, suggesting that they are subjected to less traction stress, as actin stress fibers are fundamental in generating traction against the extracellular matrix (Tanner et al., 2010). Since traction stress can alter nuclear shape (Dickinson et al., 2015), we generated a simple model of a membrane (such as the nuclear envelope) subjected to an imposed displacement of varying magnitude, representing different levels of traction stress (Fig. 5E). We observed that imposed displacements may contribute to the formation of wrinkles in the membrane, oriented along the axis of displacement (Fig. 5F, G), which is similar to the frequently seen orientation of nuclear invaginations along the longer axis of the nucleus (Figs. 4, 5A-D). Moreover, the magnitude of the wrinkles decreases with imposed displacements of lower magnitude (Fig. 5F, G). This is consistent with the hypothesis that decreased traction would lead to reduced nuclear invaginations, implying that HPV oncogenes could stabilize nuclear architecture in irradiated cells by reducing stress fiber mediated traction stress.

HPV oncogenes E6 and E7 participate in pro-survival responses, inactivating p53 and activating the PI3K/AKT signaling pathway (Scheffner et al., 1990; Zhang et al., 2015), which could oppose UVR pro-apoptotic effects. However, UVR might also reduce cell viability by affecting cell and nuclear organization (Szekely et al., 1980; Pereira et al., 2021). Our observations of decreased actin fibers and disappearance of perinuclear actin rings after UVR point in the same direction. However, our results also show less nuclear deformations after UVR in HaCaT E5/E6/E7-18 cells compared to parental cells, and our mechanical modeling points to decreased traction stress mediated by actin fibers as the cause. In our previous work, we showed that HaCaT E5/E6/E7-18 cells are softer and rounder than their parental counterparts (Millán et al., 2023). By altering the actin cytoskeleton and decreasing cell stiffness, HPV oncogenes could contribute to generate a mechanical environment that dampens perturbations in nuclear architecture, particularly in hostile conditions such as exposure to UVB radiation.

In conclusion, HPV oncogenes, likely by their effects on mechanical properties and cytoskeletal organization in human keratinocytes, contribute to maintain nuclear architecture after UVBR exposure. This, in turn, would be expected to contribute to the higher cell viability of human keratinocytes

expressing HPV oncogenes. Our current work highlights the role of HPV oncogenes in preserving cell and nuclear architecture after UVBR, leading to higher cell viability and increasing the likelihood of UVBR induced carcinogenesis.

Declarations

Declaration of Competing interest

The authors declare no competing interests.

Funding

This work was supported partially by Comisión Sectorial de Investigación Científica (CSIC)

Author Contribution

M.M, F.P., M.A., and J.H. performed the experiments. M.M., F.P., P.H., S.Y., M.A. and J.H assisted with experiments, data acquisition and analysis. J.P.Z. and M.A. developed the numerical model and J.P.Z. developed the python library and obtained the numerical results. M.A. J.H wrote the paper. All authors reviewed the manuscript.

Acknowledgement

We are grateful to Comisión Sectorial de Investigación Científica (CSIC)

Data Availability

All data supporting the findings of this study are available within the paper

References

1. Azzouz D, Khan MA, Sweezey N, Palaniyar N. Two-in-one: UV radiation simultaneously induces apoptosis and NETosis. *Cell Death Discov*. 2018;4:51. doi:10.1038/s41420-018-0048-3.
2. Beiter J, Voth GA. Making the cut: Multiscale simulation of membrane remodeling. Curr Opin Struct Biol. 2024;87:102831. doi: 10.1016/j.sbi.2024.102831.
3. Bush MA, Hermanson AS, Yetto RJ, Wieczkowski G Jr. The use of ultraviolet LED illumination for composite resin removal: an in vitro study. *Gen Dent*. 2010;58(5):e214-e218.

4. Dickinson RB, Neelam S, Lele TP. Dynamic, mechanical integration between nucleus and cell–where physics meets biology. *Nucleus*. 2015;6(5):360–365. doi:10.1080/19491034.2015.1090074.
5. Fracchia A, Asraf T, Salmon-Divon M, Gerlitz G. Increased lamin B1 levels promote cell migration by altering perinuclear actin organization. *Cells*. 2020;9(10):2161. doi:10.3390/cells9102161.
6. Gartner LP, Gartner RC. Nuclear inclusions: a study of aging in Drosophila. *J Gerontol*. 1976;31(4):396–404. doi:10.1093/geronj/31.4.396.
7. Godar DE, Tang R, Merrill SJ. Pharyngeal and cervical cancer incidences significantly correlate with personal UV doses among whites in the United States. *Anticancer Res*. 2014;34(9):4993–4999.
8. Greinert R, Volkmer B, Henning S, Breitbart EW, Greulich KO, Cardoso MC, et al. UVA-induced DNA double-strand breaks result from the repair of clustered oxidative DNA damages. *Nucleic Acids Res*. 2012;40(20):10263–10273. doi:10.1093/nar/gks824.
9. Hassouna A, Gouda I, Ismail H. Prevalence of human papilloma virus in oropharyngeal, tongue and lip squamous cell carcinoma: an experience from the Egyptian National Cancer Institute. *J Investig Med*. 2019;67(7):1061–1066. doi:10.1136/jim-2018-000968.
10. Hochmann J, Parietti F, Martínez J, Lopez AC, Carreño M, Quijano C, et al. Human papillomavirus type 18 E5 oncoprotein cooperates with E6 and E7 in promoting cell viability and invasion and in modulating the cellular redox state. *Mem Inst Oswaldo Cruz*. 2020;115:e190405. doi:10.1590/0074-02760190405.
11. Hochmann J, Millán M, Hernández P, Lafon-Hughes L, Aiuto N, Silva A, et al. Contributions of viral oncogenes of HPV-18 and hypoxia to oxidative stress and genetic damage in human keratinocytes. *Sci Rep*. 2023;13(1):17734. doi:10.1038/s41598-023-44880-3
12. Jackson S, Harwood C, Thomas M, Banks L, Storey A. Role of Bak in UV-induced apoptosis in skin cancer and abrogation by HPV E6 proteins. *Genes Dev*. 2000;14(23):3065–3073. doi:10.1101/gad.182100.
13. Janota CS, Calero-Cuenca FJ, Gomes ER. The role of the cell nucleus in mechanotransduction. *Curr Opin Cell Biol*. 2020;63:204–211. doi:10.1016/j.ceb.2020.03.001.
14. Jenkins, J.T. Static equilibrium configurations of a model red blood cell. *J. Math. Biology* 4, 149–169 (1977). https://doi.org/10.1007/BF0027598127.
15. Kanno Y, Ohsaki M. Minimum principle of complementary energy of cable networks by using second-order cone programming. *Int J Solids Struct*. 2003;40(17):4437–4460. doi:10.1016/S0020-7683(03)00215-4.
16. Kanno Y. Nonsmooth mechanics and convex optimization. 1st ed. Boca Raton: CRC Press; 2011. doi:10.1201/b10839.
17. Kreimer AR, Clifford GM, Boyle P, Franceschi S. Human papillomavirus types in head and neck squamous cell carcinomas worldwide: a systematic review. *Cancer Epidemiol Biomarkers Prev*. 2005;14(2):467–475. doi:10.1158/1055-9965.EPI-04-0551.
18. Kumar R, Deep G, Agarwal R. An overview of ultraviolet B radiation-induced skin cancer chemoprevention by silibinin. *Curr Pharmacol Rep*. 2015;1(3):206–215. doi:10.1007/s40495-015-

0027-9.

19. Leverrier S, Bergamaschi D, Ghali L, Ola A, Warnes G, Akgül B, et al. Role of HPV E6 proteins in preventing UVB-induced release of pro-apoptotic factors from the mitochondria. *Apoptosis*. 2007;12(3):549–560. doi:10.1007/s10495-006-0004-1.
20. Lewis WJ. Tension structures: form and behaviour. London: Thomas Telford Ltd; 2003.
21. McGee S, Mirkovic J, Mardirossian V, Elackattu A, Yu CC, Kabani S, et al. Model-based spectroscopic analysis of the oral cavity: impact of anatomy. *J Biomed Opt*. 2008;13(6):064034. doi:10.1117/1.2992139.
22. Millán M, Villarreal L, D'Aiuto N, Bologna-Molina R, Sotelo-Silveira J, Benech JC, et al. Mechanical profile of human keratinocytes expressing HPV-18 oncogenes. *Biochem Biophys Res Commun*. 2023;657:86–91. doi:10.1016/j.bbrc.2023.03.054.
23. Minoni L, Romero-Medina MC, Venuti A, Sirand C, Robitaille A, Altamura G, et al. Transforming properties of beta-3 human papillomavirus E6 and E7 proteins. *mSphere*. 2020;5(4):e00398-20. doi:10.1128/mSphere.00398-20.
24. Pereira NR, Russo LC, Forti FL. UV radiation-induced impairment of cellular morphology and motility is enhanced by DUSP3/VHR loss and FAK activation. *Cell Biochem Biophys*. 2021;79(2):261–269. doi:10.1007/s12013-021-00966-1
25. Scheffner M, Werness BA, Huibregtse JM, Levine AJ, Howley PM. The E6 oncoprotein encoded by human papillomavirus types 16 and 18 promotes the degradation of p53. *Cell*. 1990;63(6):1129–1136. doi:10.1016/0092-8674(90)90409-8.
26. Szekely JG, Copps TP, Morash BD. Radiation-induced invagination of the nuclear envelope. *Radiat Res*. 1980;83(3):621–632.
27. Tanner K, Boudreau A, Bissell MJ, Kumar S. Dissecting regional variations in stress fiber mechanics in living cells with laser nanosurgery. *Biophys J*. 2010;99(9):2775–2783. doi:10.1016/j.bpj.2010.08.071.
28. Tripodis N, Demant P. Genetic linkage of nuclear morphology of mouse lung tumors to the Kras-2 locus. *Exp Lung Res*. 2001;27(3):185–196.
29. Zhang HW, Zhang L, Gao Q. An efficient computational method for mechanical analysis of bimodular structures based on parametric variational principle. *Comput Struct*. 2011;89(23–24):2352–2360.
30. Zhang L, Wu J, Ling MT, Zhao L, Zhao KN. The role of the PI3K/Akt/mTOR signalling pathway in human cancers induced by infection with human papillomaviruses. *Mol Cancer*. 2015;14:87. doi:10.1186/s12943-015-0361-x

Footnotes

1. Available at: https://github.com/jorgepz/cablenets

Figures

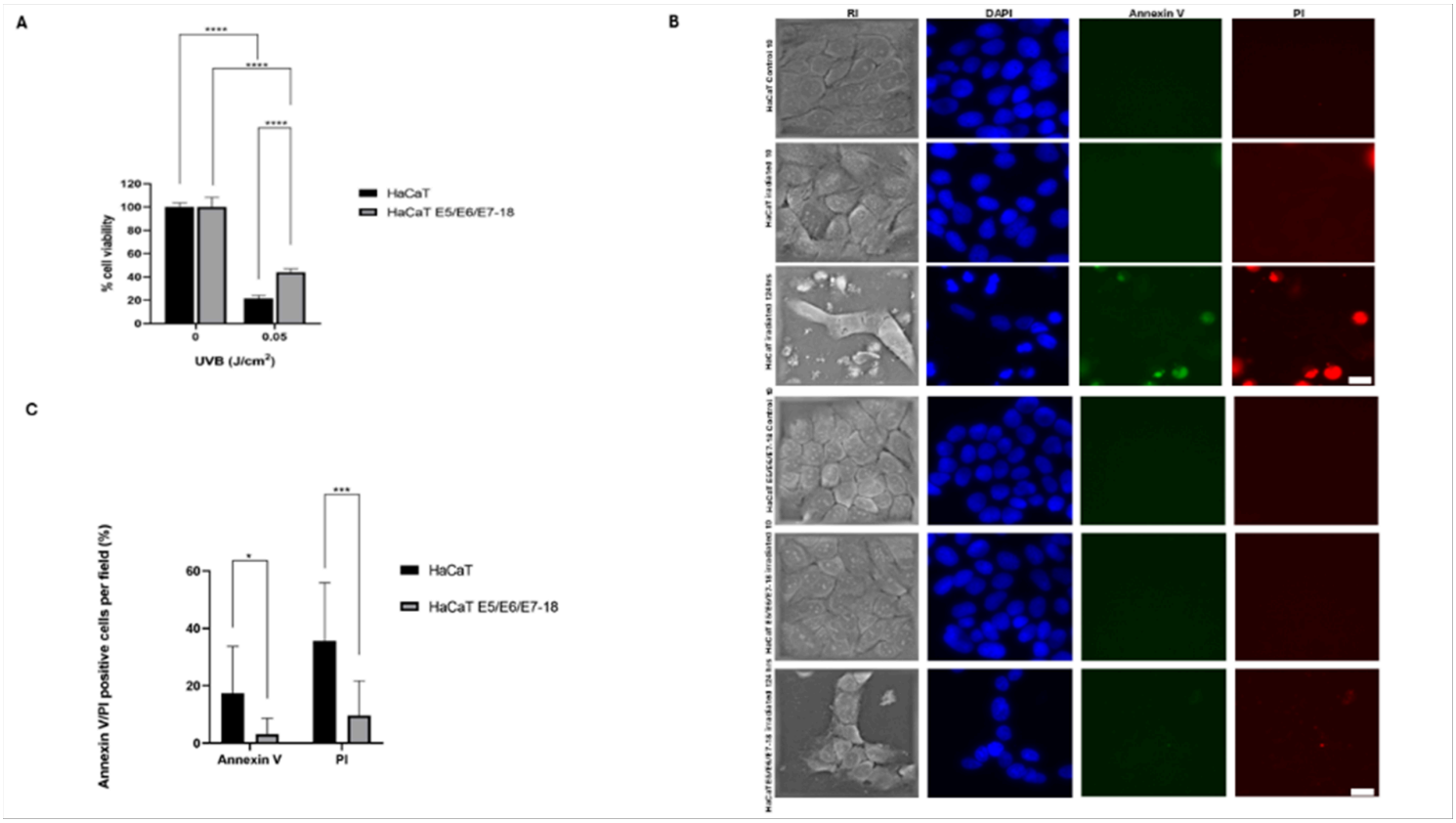

Figure 1

Cell viability and markers of apoptosis and necrosis after UVBR exposure. (A) Cell viability quantified by MTT assay in control conditions and at t0 or t24h after UVB exposure. (B). Representative images of HaCaT parental and HaCaT E5/E6/E7-18 cells, showing total number of cells per field by quantitative phase microscopy, as well as cells positive for Annexin V and PI. Scale bar: 20 µm. (C) Percentage of cells per field positive for Annexin V and PI in control conditions and at t0 or t24h after UVB exposure. Mean ± SD is shown for each cell line. For all experiments, two-way analysis of variance (ANOVA) test was conducted to assess statistical significance among groups along with Tukey's HSD test for multigroup comparison. *P < 0.05, **P < 0.01, ***P < 0.001, ****P < 0.0001.

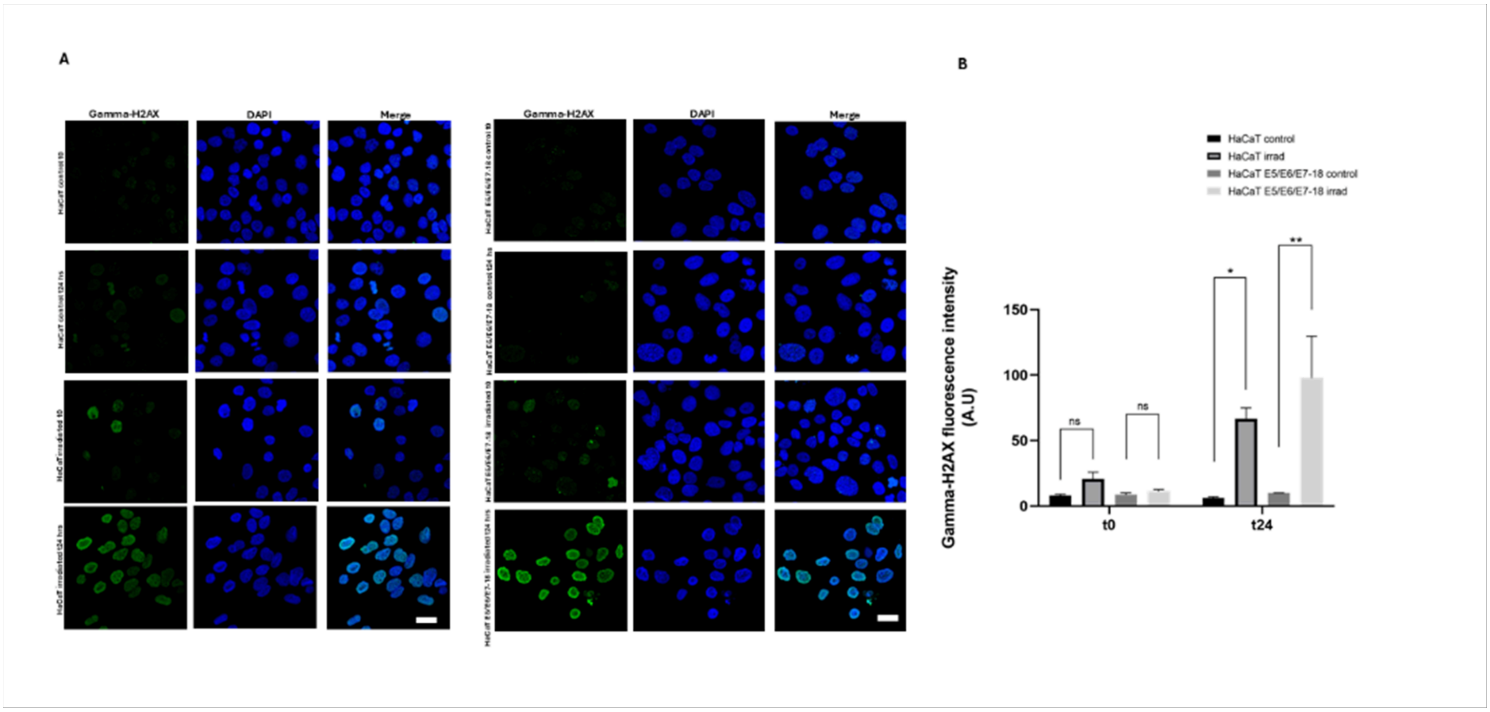

Figure 2

DNA damage levels after UVBR exposure assessed by γH2AX levels. (A, B). Representative images of γH2AX signal in parental HaCaT (A) and HaCaT E5/E6/E7-18 cells (B) irradiated at t0 and 24h after UVBR exposure and in control conditions at the same times. Scale bar: 20 μm. (C) Quantification of γH2AX intensity (mean ± SD) in parental HaCaT and HaCaT E5/E6/E7-18 cells irradiated at t0 and 24h after UVBR exposure and in control conditions at the same times. Mean ± SD is shown for each cell line. For all experiments, two-way analysis of variance (ANOVA) test was conducted to assess statistical significance among groups along with Tukey's HSD test for multigroup comparison. *P < 0.05, **P < 0.01, ***P < 0.001, ****P < 0.0001.

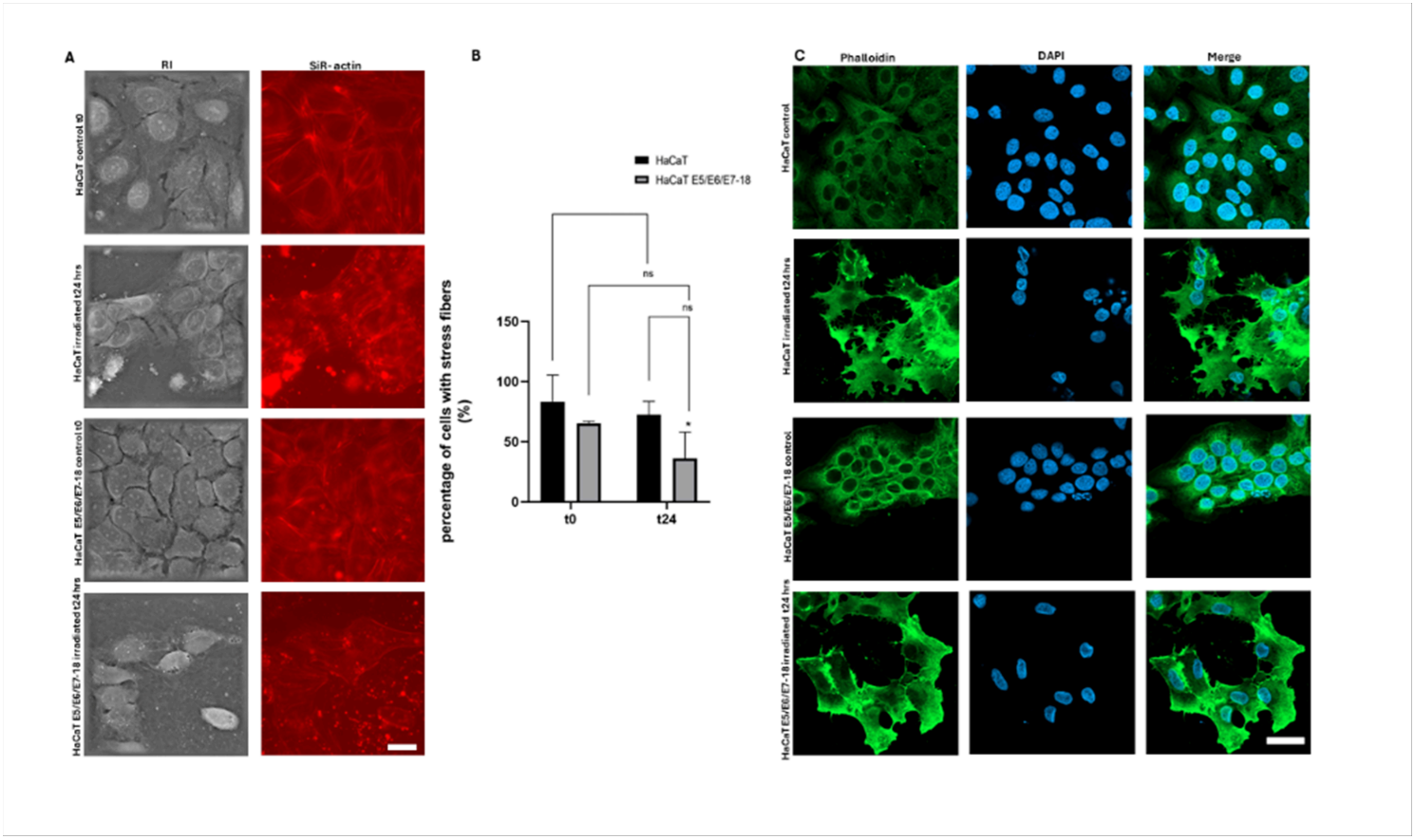

Figure 3

Changes in the actin cytoskeleton after UVBR exposure. (A) Representative images of SIR-actin signal and the corresponding quantitative phase images in live parental HaCaT and HaCaT E5/E6/E7-18 cells 24h after UVBR or in control conditions. Scale bar: 20 μm. (B) Percentage of cells with stress fibers visualized by SIR actin (mean ± SD) 24h after UVBR or in control conditions. (C) Representative images of f-actin visualized by phalloidin staining in parental HaCaT and HaCaT E5/E6/E7-18 cells 24h after UVBR or in control conditions. Scale bar: 20 μm. Two-way analysis of variance (ANOVA) test was conducted to assess statistical significance among groups along with Tukey's HSD test for multigroup comparison. *P < 0.05, **P < 0.01, ***P < 0.001, ****P < 0.0001.

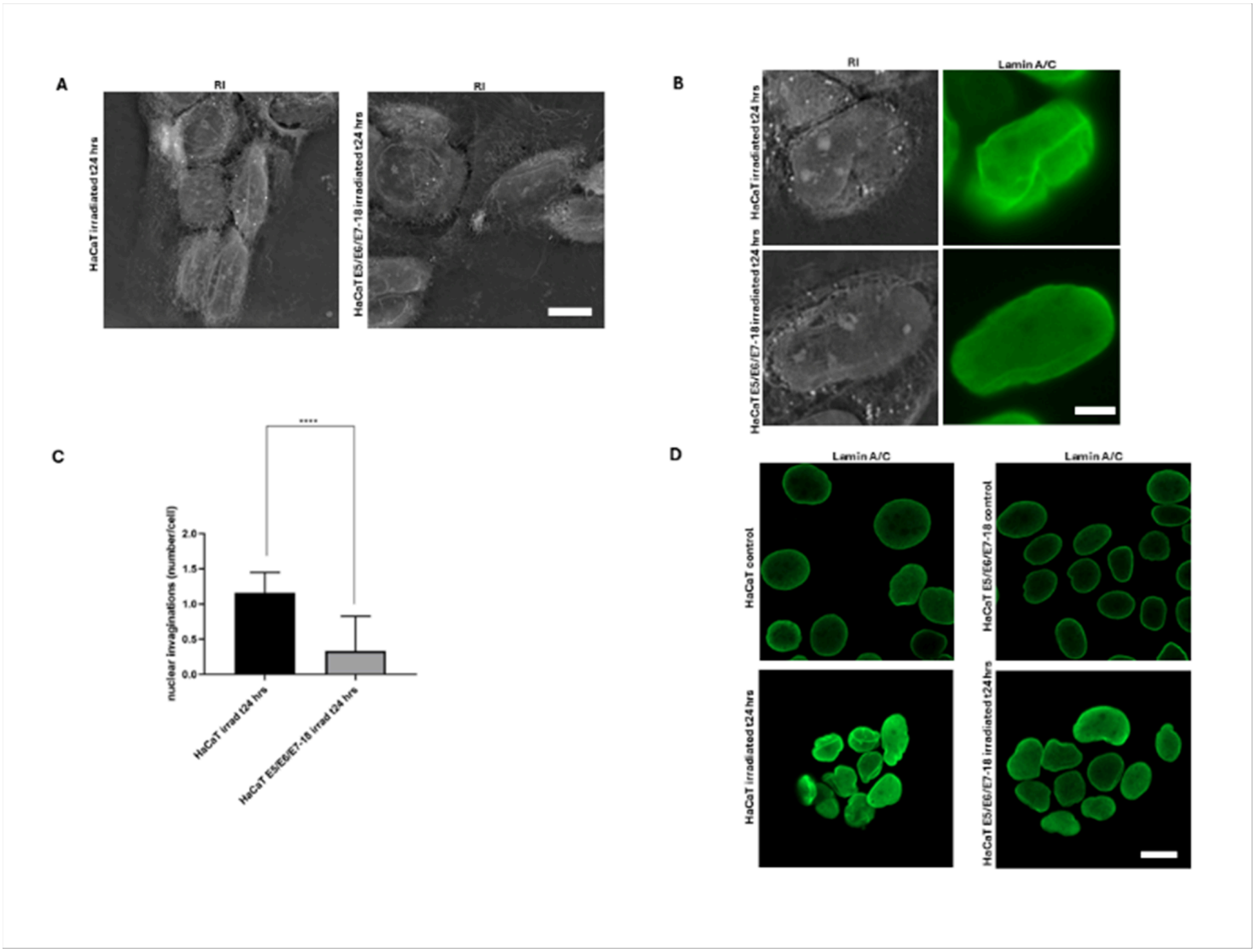

Figure 4

Nuclear lines corresponding to nuclear invaginations visualized by quantitative phase microscopy and by lamin A/C staining. (A). Representative quantitative phase images of live parental HaCaT and HaCaT E5/E6/E7-18 cells 24h after UVBR showing prominent nuclear lines. (B) Simultaneous imaging by quantitative phase microscopy and epifluorescence in parental HaCaT and HaCaT E5/E6/E7-18 cells 24h after UVBR, fixed and stained for lamin A/C. (C). Quantification of nuclear lines corresponding to nuclear invaginations in HaCaT parental and HaCaT E5/E6/E7-18 cells 24h after UVBR. Mean ± SD is shown for each cell line, and Student`s Test was conducted to assess significance. (*) $p < 0.05$, (**) $p < 0.01$, (***) $p < 0.001$. (D) Representative confocal images of lamin A/C in parental HaCaT and HaCaT E5/E6/E7-18 cells 24h after UVBR, confirming that nuclear lines display strong lamin A/C signal. Scale bars: 20 µm.

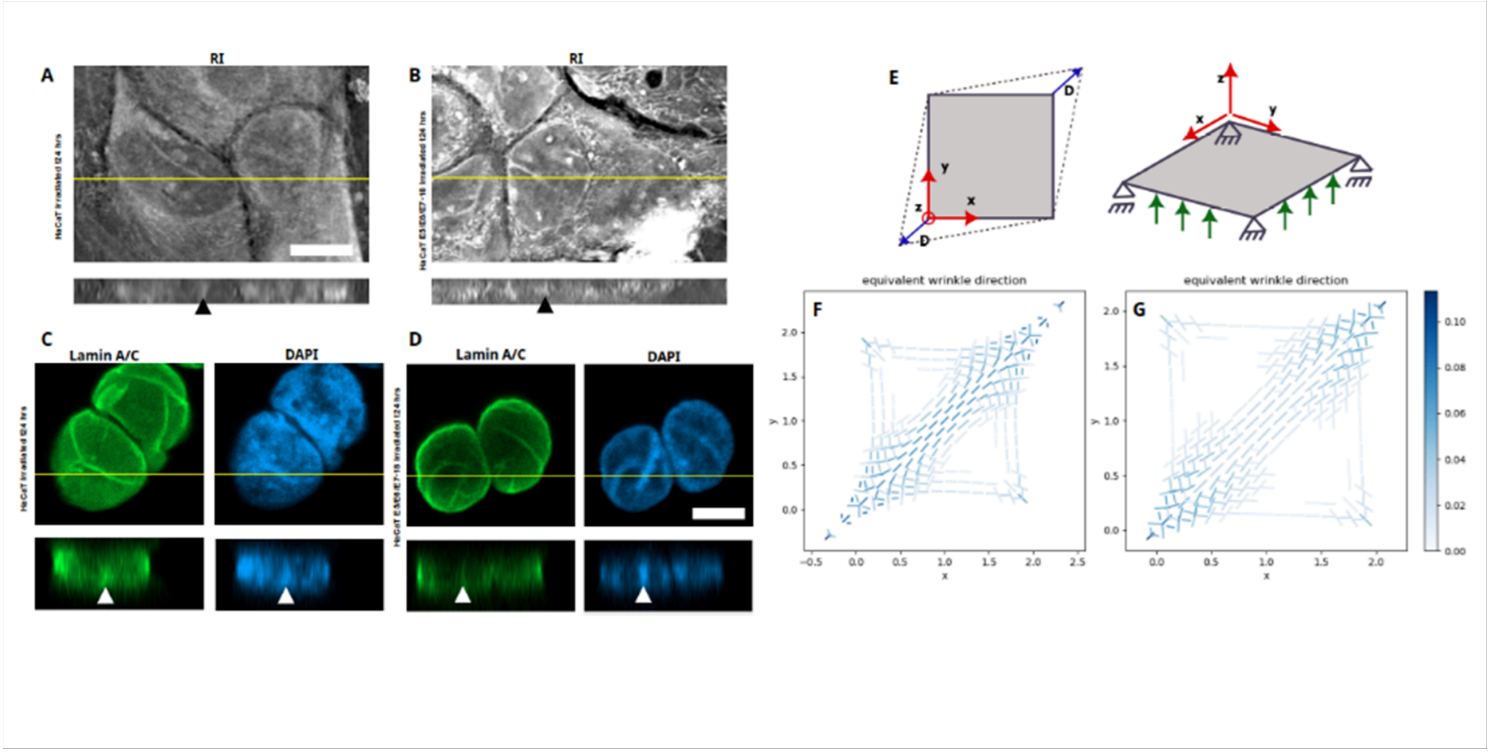

Figure 5

Nuclear lines correspond to nuclear invaginations, which can be caused by traction forces. (A and B). Quantitative phase images of HaCaT parental (A) and HaCaT E5/E6/E7-18 cells (B) 24h after UVBR showing nuclear lines, accompanied by their respective xz reconstructions, indicating that nuclear lines correspond to nuclear invaginations often spanning the entire depth of the nucleus (arrows). (C and D). Confocal images of HaCaT parental (C) and HaCaT E5/E6/E7-18 cells (D) 24h after UVBR, showing nuclear lines with strong lamin A/C and DAPI signals, accompanied by their respective xz reconstructions, which also show deep nuclear invaginations (arrows). (E) A membrane modelled as a network of interconnected cables is subjected to traction forces: a square domain is considered, where the plane x-y cablenet is subjected to a uniform distributed force in z (green arrows) and imposed displacements D in two vertices (blue arrows), (F, G) This imposed displacement creates wrinkles in the membrane (equivalent to nuclear invaginations), color coded for magnitude and of the indicated direction. (F) Imposed displacement of 60% diagonal stretch. (G) Imposed displacement of 20% diagonal stretch. Wrinkles decrease in magnitude with decreased imposed displacement. Scale bars: 10 μm.